Third-order Complex Amplitudes Tracking Loop for Slow Flat Fading Channel On-Line Estimation

Huaqiang Shu, Laurent Ros, Eric Pierre Simon

Third-order Complex Amplitudes Tracking Loop for Slow Flat Fading Channel On-Line Estimation *

Huaqiang Shu, Laurent Ros, and Eric Pierre Simon †

***Abstract*—This paper deals with channel estimation in tracking mode over a flat Rayleigh fading channel with Jakes' Doppler Spectrum. Many estimation algorithms exploit the time-domain correlation of the channel by employing a Kalman filter based on a first-order (or sometimes second-order) approximation model of the time-varying channel. However, the nature of the approximation model itself degrades the estimation performance for slow to moderate varying channel scenarios. Furthermore, the Kalman-based algorithms exhibit a certain complexity. Hence, a different model and approach has been investigated in this work to tackle all of these issues. A novel PLL-structured third-order tracking loop estimator with a low complexity is proposed. The connection between a steady-state Kalman filter based on a random walk approximation model and the proposed estimator is first established. Then, a sub-optimal mean-squared-error (MSE) is given in a closed-form expression as a function of the tracking loop parameters. The parameters that minimize this sub-optimal MSE are also given in a closed-form expression. The asymptotic MSE and Bit-Error-Ratio (BER) simulation results demonstrate that the proposed estimator outperforms the first and second order Kalman-based filters reported in literature. The robustness of the proposed estimator is also verified by a mismatch simulation.**

***Index Terms*—Channel estimation, Rayleigh fading, Jakes' spectrum, Random Walk model (RW), Phase-locked loop (PLL), Kalman filter (KF).**

I. Introduction

Channel estimation is a fundamental task for a wireless communication receiver. This paper deals with channel path Complex Amplitude (CA) estimators in tracking mode. The statistical channel model assumed in this paper to describe the wireless channel is the Rayleigh fading channel with Jakes' Doppler spectrum model [2] (also called the Clarke Model [3]). It is widely accepted in the literature for frequency-flat correlated fading channels.

Many channel path CA tracking algorithms use a Kalman filter (KF). KF-based algorithms exhibit a certain complexity and the design of a KF requires to dispose of a linear recursive state-space representation of the channel. However, the exact Clarke model does not admit such a representation. An approximation often employed in the literature consists of approaching the fading process as Auto-Regressive (AR) [4], in the perspective to design a KF [5]–[11]. The larger the order of the model, the better the approximation of the actual fading statistics, but also the larger the complexity. So, despite its complexity, KF-based algorithms do not ensure optimal performance if the structure or the tuning of the approximation model are not well suited, as developed hereafter. A widely used channel approximation model results from a first-order Auto-Regressive model (AR1) as recommended by [12], combined with a Correlation Matching (CM) criterion to fix the AR1-coefficient (equal then to the standard Bessel AR1-coefficient, $J_0(2\pi f_d T)$, for a given normalized Doppler frequency $f_d T$). The KF channel estimator resulting from this choice, called AR1$_{CM}$-KF in this paper, was used in several papers concerning various systems such as in Multiple-Input-Multiple-Output (MIMO) systems [5], [6], or in Orthogonal Frequency Division Multiplexing (OFDM) systems [7], [8], [13], [14]. The AR1$_{CM}$-KF seems to be convenient for the very high mobility case, leading to quasi-optimal channel estimation performance compared to lower bounds, as seen, for example, in [13]–[15] (in these works the AR1$_{CM}$-KF is actually used to track the Basis Extension Model coefficients of the high speed channel). But for most conventional Doppler speeds whereby the channel variation within one symbol duration can be neglected ($i.e.$ $f_d T \leq 10^{-2}$, as in [5]–[11], [16]), the AR1$_{CM}$-KF estimator usually exploited in the literature is far from being effective [9]. This poor performance has been recently explained analytically in [10], mainly because the CM criterion is shown to be inappropriate to tune the AR1-coefficient in slow or moderate fading scenario (since the choice of $J_0(2\pi f_d T) \approx 1 - \frac{1}{4}(2\pi f_d T)^2$ for the AR1 coefficient is too close to the value 1 to ensure a good trade-off between tracking ability and noise mitigation). A better tuning of the AR1-coefficient can focus on minimizing the estimation variance in output of the KF as proposed in [9] (with analytic MSE performance for a given Doppler and Signal-to-Noise Ratio (SNR) scenario in [10]), $i.e.$ using a minimum asymptotic variance (MAV) criterion without imposing the CM constraint. The resulting estimator is called AR1$_{MAV}$-KF in this paper.

On the other hand, [11] analytically shows that the MSE performance of a KF can still be improved by switching from the AR1 model to an integrated random walk (RW) model (also called integrated Brownian model) for the approximation model. Such a model was a second-order approximation model that better takes into account the fact that the exact channel CA continues in a given direction during several symbols for low $f_d T$ and then exhibits a strong trend behaviour. The Kalman estimator based on this special second-order model is called RW2-KF in this paper.

*Part of this work was presented in the conference ICT2012 [1]

†H. Shu and E. P. Simon are with IEMN lab, TELICE group, 59655 Villeneuve d'Ascq, France. L. Ros is with GIPSA-Lab, Image and Signal Department, BP 46, 38402 Saint Martin d'Hères, France.

So far, all our discussion dealt with KF-based algorithms, but we now wish to obtain simpler adaptive algorithms. This can be done by deriving steady-state versions of the KF based on a random-walk (RW) approximation model, yielding a recursive linear filter with constant coefficients. In general, such algorithms converge slower than the KF, but can reach the same asymptotic performance in tracking mode. To start with, we should bear in mind that the LMS algorithm, which is the most popular adaptive algorithm, can be viewed as a steady-state version of a KF based on a first-order RW approximation model [17]. The second-order LMS was first proposed by [18] in a channel estimation context. It was derived as the steady-state version of a KF based on a second-order integrated RW approximation model (RW2-KF). However, the author does not specify how to tune the two constant coefficients of the model. [19] proposed a method to obtain optimal coefficients, and [16], [20] presented the CA tracking algorithm and its optimization from a second-order phase-locked-loop (PLL) point of view. Indeed, as it has been already shown by Driessen [21] and Christiansen [22] in the case of the phase estimation problem, a proportional-integral (second-order) PLL has the same structure as the KF when considering the second-order integrated RW model, and thereafter the closed-form Kalman gain expression is given in [23]. The algorithm of [16], [20] is called the second-order complex amplitude tracking loop (RW2-CATL).

In this paper, we propose and study a low-complexity flat fading channel estimator based on a third-order integrated RW model (RW3). The contributions of this paper are multi-fold with the purpose to solve the following questions: Why could a PLL-structured estimator asymptotically work like a traditional one (*e.g.* a KF) ? What is the relationship between them ? How much can a well-chosen *third-order* CATL outperform, in terms of asymptotic MSE performance, the more complex KF based only on *first-* or *second*-order models (*e.g.* AR1$_{CM}$-KF, AR1$_{MAV}$-KF, or RW2-KF) ? How to tune properly and in a simple way the coefficients of such a third-order CATL, assuming Rayleigh-Jakes channel and a given scenario of f_dT and SNR? What is then the closed form expression of the MSE of such a channel estimator ? How does a distorted foreknowledge of Doppler frequency or noise power information influence the estimator performance ?

Section II gives the system model. In section III, we propose and analyze a third-order Complex-Amplitude-Tracking Loop, called RW3-CATL, for the time-varying channel estimation. Section IV describes the proposed method to correctly tune the loop coefficients, and section V validates our model and assumptions by means of MSE and BER simulations.

II. Model and Estimation Objective

We consider the estimation of a flat Rayleigh fading channel in a digital modulation system. The discrete-time observation is:

$$r_{(n)} = \alpha_{(n)} \cdot x_{(n)} + v_{(n)}, \tag{1}$$

where n is the symbol time index; $x_{(n)} = a_{(n)} + jb_{(n)}$ with $a_{(n)}, b_{(n)} \in \Re$ is the transmitted phase modulated (M-PSK) or quadrature amplitude modulation (M-QAM) symbol, the sequence of transmitted symbol is assumed to be zero-mean and stationary with normalized variance : $E\left\{\left|x_{(n)}\right|^2\right\} = \sigma_x^2 = 1$; $v_{(n)}$ is a zero-mean additive white circular complex Gaussian noise with variance σ_v^2; and $\alpha_{(n)}$ is a zero-mean circular Gaussian channel Complex Amplitude with variance σ_α^2. Note that this model can be applied to more advanced systems such as OFDM system, where α would then represent the channel gain to be estimated at one pilot frequency as in [7], and $x_{(n)}$ could then be a known (or pilot) symbol in the channel estimation perspective (data-aided scenario).

The normalized Doppler frequency of this channel is f_dT, where f_d is the Doppler frequency and T is the symbol period. A Jakes' Doppler spectrum is assumed for this channel:

$$\Gamma_\alpha(f) = \begin{cases} \frac{\sigma_\alpha^2}{\pi f_d \sqrt{1-\left(\frac{f}{f_d}\right)^2}}, & \text{if} \quad |f| < f_d \\ 0, & \text{if} \quad |f| \geq f_d. \end{cases} \tag{2}$$

The autocorrelation coefficient of the stationary CA α is then defined for lag q by:

$$R_\alpha[q] = E\left\{\alpha_{(n)} \cdot {\alpha_{(n-q)}}^*\right\} = \sigma_\alpha^2 J_0(2\pi f_d T \cdot q), \tag{3}$$

where J_0 is the zeroth-order Bessel function of the first kind. Given the observation model (1) and the Doppler spectrum statistical constraint (2) for the dynamic evolution of the CA, we look for an on-line unbiased estimation $\hat{\alpha}_{(n)}$ of $\alpha_{(n)}$. The MSE $\sigma_\epsilon^2 \overset{\text{def}}{=} E\left\{\left|\epsilon_{(n)}\right|^2\right\}$ of the estimation error $\epsilon_{(n)} \overset{\text{def}}{=} \alpha_{(n)} - \hat{\alpha}_{(n)}$ will be investigated.

III. Complex Amplitude Tracking Loop

A. From steady-state KF to PLL-structured CATL

1) RW3 model and RW3-KF: similar to the method presented in [18], in the slow to moderate fading scenario, we can firstly depict a steady-state KF [24], but based here on a RW3 model, denoted as RW3-KF. The model can be formulated in discrete time update equations as:

$$\tilde{\alpha}_{(n)} = \tilde{\alpha}_{(n-1)} + \delta_{(n-1)} + \frac{1}{2}\xi_{(n-1)}, \tag{4}$$

$$\delta_{(n)} = \delta_{(n-1)} + \xi_{(n-1)}, \tag{5}$$

$$\xi_{(n)} = \xi_{(n-1)} + u_{(n)}, \tag{6}$$

where $u_{(n)}$ is a zero mean circular complex Gaussian with variance σ_u^2. The equation (4) is the discrete version of the Taylor series expansion of a continuous signal. So in this approximation model, the approximate process of $\alpha_{(n)}$, denoted $\tilde{\alpha}_{(n)}$, is updated by a time increment of $\delta_{(n-1)} + \frac{1}{2}\xi_{(n-1)}$ every symbol period with $\delta_{(n)}$ and $\xi_{(n)}$ respectively approximate the first- and second-order derivative of the continuous signal. The observation model is given by (1), which could be rewritten in separating the parameter $\alpha_{(n)}$ from the transmitted signal as:

$$y_{(n)} = \alpha_{(n)} + \mathrm{w}_{(n)}, \tag{7}$$

with $y_{(n)} = \frac{r_{(n)}}{x_{(n)}}$ and $\mathrm{w}_{(n)} = \frac{v_{(n)}}{x_{(n)}}$. Note that $\mathrm{w}_{(n)}$ remains a zero-mean additive white circular complex noise with variance $\sigma_{\mathrm{w}}^2 = K_{\mathrm{mod}} \cdot \sigma_v^2$ where $K_{\mathrm{mod}} = E\left\{\left|\frac{1}{x_{(n)}}\right|^2\right\}$ is a constant

factor, known for a given modulation scheme. For a special case of constant-energy modulation, *e.g.* M-PSK, we would have $\sigma_{\text{w}}^2 = \sigma_v^2$ and $K_{\text{mod}} = 1$. Then we reform (7) and (4)$\sim$(6) in matrix form as:

$$y_{(n)} = \mathbf{S}\boldsymbol{a}_{(n)} + \text{w}_{(n)}, \tag{8}$$

$$\boldsymbol{a}_{(n)} = \mathbf{M}\boldsymbol{a}_{(n-1)} + \mathbf{u}_{(n)}, \tag{9}$$

with the selection vector $\mathbf{S} = \begin{bmatrix}1 & 0 & 0\end{bmatrix}$, the state vector $\boldsymbol{a}_{(n)} \overset{\text{def}}{=} \begin{bmatrix}\tilde{\alpha}_{(n)} & \delta_{(n)} & \xi_{(n)}\end{bmatrix}^T$, the state noise vector $\mathbf{u}_{(n)} = \begin{bmatrix}0 & 0 & u_{(n)}\end{bmatrix}^T$ and the 3×3 evolution matrix $\mathbf{M} = \begin{bmatrix}1 & 1 & \frac{1}{2}; & 0 & 1 & 1; & 0 & 0 & 1\end{bmatrix}$. The observation equation (8) and the state evolution equation (9) compose the state-space model of the KF. The corresponding two-stage KF equations are then written as:

Time Update Equations

$$\hat{\boldsymbol{a}}_{(n|n-1)} = \mathbf{M}\hat{\boldsymbol{a}}_{(n-1|n-1)}, \tag{10}$$

$$\mathbf{P}_{(n|n-1)} = \mathbf{M}\mathbf{P}_{(n-1|n-1)}\mathbf{M}^T + \mathbf{U}, \tag{11}$$

Measurement Update Equations

$$\mathbf{K}_{(n)} = \frac{\mathbf{P}_{(n|n-1)}\mathbf{S}^T}{\mathbf{S}\mathbf{P}_{(n|n-1)}\mathbf{S}^T + \sigma_{\text{w}}^2}, \tag{12}$$

$$\hat{\boldsymbol{a}}_{(n|n)} = \hat{\boldsymbol{a}}_{(n|n-1)} + \mathbf{K}_{(n)}(y_{(n)} - \mathbf{S}\hat{\boldsymbol{a}}_{(n|n-1)}), \tag{13}$$

$$\mathbf{P}_{(n|n)} = (\mathbf{I} - \mathbf{K}_{(n)}\mathbf{S})\mathbf{P}_{(n|n-1)}, \tag{14}$$

with $\hat{\boldsymbol{a}}_{(n|n-1)} \overset{\text{def}}{=} \begin{bmatrix}\hat{\alpha}_{(n|n-1)} & \hat{\delta}_{(n|n-1)} & \hat{\xi}_{(n|n-1)}\end{bmatrix}^T$ the prediction of state vector, $\hat{\boldsymbol{a}}_{(n|n)} \overset{\text{def}}{=} \begin{bmatrix}\hat{\alpha}_{(n|n)} & \hat{\delta}_{(n|n)} & \hat{\xi}_{(n|n)}\end{bmatrix}^T$ the estimation of state vector, and the 3×3 state noise matrix is defined as $\mathbf{U} = \begin{bmatrix}0 & 0 & 0; & 0 & 0 & 0; & 0 & 0 & \sigma_u^2\end{bmatrix}$, $\mathbf{K}_{(n)}$ is the Kalman gain vector, $\mathbf{P}_{(n|n-1)}$, $\mathbf{P}_{(n|n)}$ are respectively the covariance matrices (both 3×3) of the prediction error and the estimation error. Define also the error signal as:

$$v_{\epsilon(n)} = y_{(n)} - \mathbf{S}\hat{\boldsymbol{a}}_{(n|n-1)}. \tag{15}$$

Note that the computation of the error signal requires the knowledge of $x_{(n)}$ since $y_{(n)}$ is the equalized version of the received signal $r_{(n)}$. Two different scenarios can then be considered : either treat $x_{(n)}$ as pilot symbols, or use the decisions instead. In the decision-directed scenario,$x_{(n)}$ is replaced by the *a priori* decision $\hat{x}_{(n|n-1)}$ to compute $y_{(n)} = \frac{r_{(n)}}{\hat{x}_{(n|n-1)}}$, where $\hat{x}_{(n|n-1)}$ is decided from the previous estimation of the channel. The value of $\hat{x}_{(n|n-1)}$ depends on the applied modulation schemes, *e.g.* in QPSK modulation, $\hat{x}_{(n|n-1)} = \frac{\sqrt{2}}{2}\cdot\text{sgn}\{\mathfrak{Re}(\hat{\alpha}^*_{(n|n-1)}\cdot r_{(n)})\} + j\frac{\sqrt{2}}{2}\cdot\text{sgn}\{\mathfrak{Im}(\hat{\alpha}^*_{(n|n-1)}\cdot r_{(n)})\}$, with $\text{sgn}\{\cdot\}$ the sign function. In this work, we concentrate on the performance of the channel estimator[1]. So the theoretical analysis is derived assuming symbols are known (pilot-aided scenario) or perfectly decided, and the effect of decision error (in the decision-directed scenario) will be observed in the simulation part.

[1]Note that in practice, our channel estimator can easily be coupled with an efficient detector in order to perform joint channel estimation and decision tasks, for example via the Expectation-Maximization algorithm framework (see [8]). In another already mentioned context, it can simply also be used to track the channel gain at pilot frequencies in an OFDM system as in [7].

2) Time-domain equations of the steady-state RW3-KF: Since the linear model ((9)(8)) is *observable* and *controllable* [25], an asymptotic regime is quickly reached [24]. In other words, $\mathbf{K}_{(n)}$ converges to a constant when n is large enough, *i.e.*

$$\mathbf{K}_{(n)} = \mathbf{K}_{(n+1)} = \mathbf{K}_{(\infty)} \overset{\text{def}}{=} \begin{bmatrix}k_1 & k_2 & k_3\end{bmatrix}^T. \tag{16}$$

By combining (10) and (13), we obtain the measurement update equations of $\hat{\alpha}$ with the steady-state RW3-KF:

$$\hat{\alpha}_{(n|n)} = \hat{\alpha}_{(n-1|n-1)} + \hat{\delta}_{(n-1|n-1)} + \frac{1}{2}\hat{\xi}_{(n-1|n-1)} + k_1 v_{\epsilon(n)}, \tag{17}$$

$$\hat{\delta}_{(n|n)} = \hat{\delta}_{(n-1|n-1)} + \hat{\xi}_{(n-1|n-1)} + k_2 v_{\epsilon(n)} \tag{18}$$

$$\hat{\xi}_{(n|n)} = \hat{\xi}_{(n-1|n-1)} + k_3 v_{\epsilon(n)}, \tag{19}$$

with $v_{\epsilon(n)}$ defined by (15).

3) The steady-state RW3-KF as an RW3-CATL: Note that k_2 and k_3 are embedded in the derivatives of the CA in (17), this makes it difficult to control directly the estimator through the use of the gains. It is however interesting to note that if we study these equations in Z-domain, the gains can be separated from the variables, and this allows us to analyse the estimator as a PLL-structured tracking loop with a PII filter (or Proportional-double-Integral filter). The expression of (17)(18)(19) in Z-domain are:

$$\hat{\alpha}(z)(1 - z^{-1}) = \hat{\delta}(z)z^{-1} + \frac{1}{2}\hat{\xi}(z)z^{-1} + k_1 v_\epsilon(z), \tag{20}$$

$$\hat{\delta}(z)(1 - z^{-1}) = \hat{\xi}(z)z^{-1} + k_2 v_\epsilon(z), \tag{21}$$

$$\hat{\xi}(z)(1 - z^{-1}) = k_3 v_\epsilon(z). \tag{22}$$

Substituting (21)(22) in (20), we have:

$$\hat{\alpha}(z)(1-z^{-1}) = \left[k_1 + \frac{(k_2 + \frac{1}{2}k_3)z^{-1}}{1 - z^{-1}} + \frac{k_3 z^{-2}}{(1 - z^{-1})^2}\right] v_\epsilon(z), \tag{23}$$

The equation (23) shows the final estimate $\hat{\alpha}$ as a filtered version of the error signal v_ϵ, as in a PLL. Let us define:

$$\mu_1 = k_1, \tag{24}$$

$$\mu_2 = k_2 + \frac{1}{2}k_3, \tag{25}$$

$$\mu_3 = k_3, \tag{26}$$

and

$$v_{\text{Lag1}}(z) = \frac{v_\epsilon(z)}{1 - z^{-1}}, \tag{27}$$

$$v_{\text{Lag2}}(z) = \frac{v_\epsilon(z)}{(1 - z^{-1})^2}, \tag{28}$$

(23) can then be rewritten as:

$$\hat{\alpha}(z)(1 - z^{-1}) = \mu_1 v_\epsilon(z) + \mu_2 v_{\text{Lag1}}(z)z^{-1} + \mu_3 v_{\text{Lag2}}(z)z^{-2}, \tag{29}$$

or equivalently in discrete-time domain:

$$\hat{\alpha}_{(n|n)} = \hat{\alpha}_{(n-1|n-1)} + \mu_1 v_{\epsilon(n)} + \mu_2 v_{\text{Lag1}(n-1)} + \mu_3 v_{\text{Lag2}(n-2)}. \tag{30}$$

From (13), we have:

$$\hat{\alpha}_{(n|n)} = \hat{\alpha}_{(n|n-1)} \ + \ k_1 v_{\epsilon(n)}. \tag{31}$$

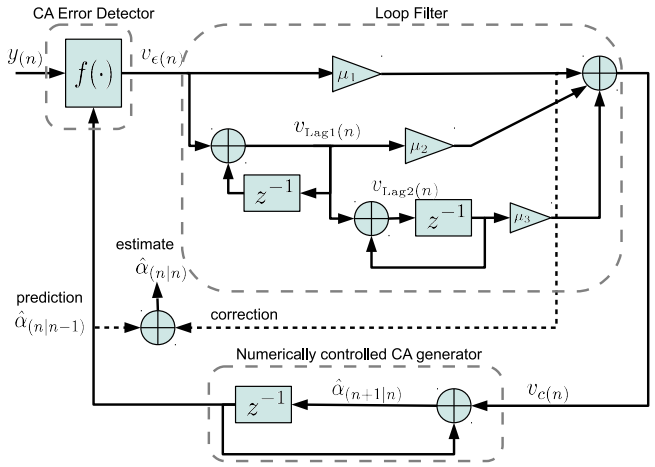

Fig. 1: Equivalent structure of the RW3-CATL

By combining (30), (31) and (24), we get the prediction equation:

$$\hat{\alpha}_{(n+1|n)} = \hat{\alpha}_{(n|n)} + \mu_2 v_{\text{Lag1}(n)} + \mu_3 v_{\text{Lag2}(n-1)}. \tag{32}$$

These equations, derived from the steady-state RW3-KF, can be slightly rearranged to resemble the most traditional form of a PLL-like structure, as shown in the next subsection.

4) Final time-domain equations of the RW3-CATL: We can now easily sum up the equations of the proposed third-order Complex Amplitude Tracking Loop (CATL), as:

Error signal:

$$v_{\epsilon(n)} = y_{(n)} - \hat{\alpha}_{(n|n-1)}, \tag{33}$$

Loop Filter:

$$v_{\text{Lag1}(n)} = v_{\text{Lag1}(n-1)} + v_{\epsilon(n)}, \tag{34}$$

$$v_{\text{Lag2}(n)} = v_{\text{Lag2}(n-1)} + v_{\text{Lag1}(n)}, \tag{35}$$

$$v_{c(n)} = \mu_1 v_{\epsilon(n)} + \mu_2 v_{\text{Lag1}(n)} + \mu_3 v_{\text{Lag2}(n-1)}, \tag{36}$$

Numerically Controlled Generator:

$$\hat{\alpha}_{(n+1|n)} = \hat{\alpha}_{(n|n-1)} \ + \ v_{c(n)}, \tag{37}$$

Final estimate:

$$\hat{\alpha}_{(n|n)} = \hat{\alpha}_{(n|n-1)} + \mu_1 v_{\epsilon(n)}. \tag{38}$$

Here (33) is from (15), (38) is obtained from (31) using (24), (34) and (35) are respectively a result of (27) and (28), and finally (36) and (37) are derived from (32) using (38).

The structure of our PLL-like estimator based on the discrete-time equations (33)∼(37) is shown in Fig.1. As in a digital PLL, the RW3-CATL is composed of an error detector, a loop filter and a numerically controlled generator.

The error detector compares firstly the received signal with a reference signal equal to the previous prediction of the parameter, $\hat{\alpha}_{(n|n-1)}$. It delivers the error signal $v_{\epsilon(n)}$ to the proportional-double-integral filter $F_{PII}(z) = \mu_1 + \frac{\mu_2}{1-z^{-1}} + \frac{\mu_3 z^{-1}}{(1-z^{-1})^2}$ which is controlled by the three filter coefficients μ_1, μ_2 and μ_3. As the steady-state Kalman gains are real positive (this can be proved by solving the Ricatti equations), the loop filter coefficients μ_1, μ_2, μ_3 are also real positive values. The signals $v_{\text{Lag1}(n)}$, $v_{\text{Lag2}(n)}$ defined in (34) and (35) are respectively the first-order and the second-order digital integrations (or accumulations) of the error signal $v_{\epsilon(n)}$. The loop filter output $v_{c(n)}$ is then used as a command by the numerically controlled generator to generate the next prediction $\hat{\alpha}_{(n+1|n)}$ from the previous one $\hat{\alpha}_{(n|n-1)}$, according to the integration process (37).

This structure is similar to the one presented in [1][2], which is deduced from a standard third-order DPLL [26]. We will also demonstrate the equivalence between the RW3-CATL and the standard third-order DPLL in the following analysis. However, unlike the conventional PLL, the final output of the CATL is not the prediction (or *a priori* estimate) $\hat{\alpha}_{(n|n-1)}$ but the final (or *a posteriori*) estimate of the complex amplitude $\hat{\alpha}_{(n|n)}$, according to equation (38), as in the KF principle. Thus an additional correction branch is added, represented by the dashed line in Fig.1. The RW3-CATL is a time-invariant filter, it hence does not need to update its coefficients. On the contrary, the RW3-KF has to update its coefficients (the Kalman gain and the error variances) every symbol period.

Note that, thanks to the second integration in $v_{\text{Lag2}(n)}$, this digital third-order loop does not exhibit acceleration-dependent steady-state error in the case of second-order variations of the CAs. In other words, the RW3-CATL characterizes the variation of the channel parameter by taking into account its slope and its curvature, while second-order loops only consider the slope.

B. General properties

1) Closed-loop transfer function of RW3-CATL: By combining (7) and (15), we have:

$$v_{\epsilon(n)} = \alpha_{(n)} - \hat{\alpha}_{(n|n-1)} + \mathrm{w}_{(n)}. \tag{39}$$

The error signal is thus a combination of the prediction error $(\alpha_{(n)} - \hat{\alpha}_{(n|n-1)})$ and the channel noise. By combining (38) and (39), we obtain the error signal - estimation error relation:

$$v_{\epsilon(n)} = \frac{1}{1-\mu_1} \cdot (\alpha_{(n)} - \hat{\alpha}_{(n|n)}) + \frac{1}{1-\mu_1} \cdot \mathrm{w}_{(n)}. \tag{40}$$

Transform (40) to the Z-domain:

$$v_{\epsilon}(z) = \frac{1}{1-\mu_1} \cdot (\alpha(z) - \hat{\alpha}(z)) + \frac{1}{1-\mu_1} \cdot \mathrm{w}(z). \tag{41}$$

By combining (27)(28)(29), we get:

$$\hat{\alpha}(z)(1-z^{-1}) = [\mu_1 + \frac{\mu_2 \cdot z^{-1}}{1-z^{-1}} + \frac{\mu_3 \cdot z^{-2}}{(1-z^{-1})^2}] \cdot v_{\epsilon}(z). \tag{42}$$

Then substituting (41) in (42) leads to:

$$\hat{\alpha}(z) = L(z) \cdot \alpha(z) + L(z) \cdot \mathrm{w}(z), \tag{43}$$

where $L(z)$ is the Z-domain transfer function of the 3rd-order CATL defined by (44) with $F(z) = \mu_1 + \frac{\mu_2 \cdot z^{-1}}{1-z^{-1}} + \frac{\mu_3 \cdot z^{-2}}{(1-z^{-1})^2}$.

[2]The proposed estimator (denoted Or3-CATL) in [1] is similar to the one of this paper, but they stem from different structures, the Or3-CATL is given directly from the third-order DPLL while the RW3-CATL is deduced from a RW3-KF; Comparing with the structure of Or3-CATL (Fig.1 of [1]), we could also find a difference between the loop filters.

$$L(z) = \frac{F(z)}{(1-\mu_1)(1-z^{-1}) + F(z)} = \frac{\left[(\mu_1-\mu_2+\mu_3)(1-z^{-1})^2 + (\mu_2-2\mu_3)(1-z^{-1}) + \mu_3\right]}{(1-\mu_1)(1-z^{-1})^3 + \left[(\mu_1-\mu_2+\mu_3)(1-z^{-1})^2 + (\mu_2-2\mu_3)(1-z^{-1}) + \mu_3\right]} \tag{44}$$

$$L(z) = \frac{(m+2)\zeta\omega_n T\cdot(1-z^{-1})^2 + (1+2m\zeta^2)(\omega_n T)^2\cdot(1-z^{-1}) + m\zeta(\omega_n T)^3}{(1-z^{-1})^3 + (m+2)\zeta\omega_n T\cdot(1-z^{-1})^2 + (1+2m\zeta^2)(\omega_n T)^2\cdot(1-z^{-1}) + m\zeta(\omega_n T)^3} \tag{45}$$

In order to be able to compare with a classic analog third-order PLL, $L(z)$ can be rewritten in a more interpretable form [3] in (45) as a function of the natural pulsation $\omega_n = 2\pi f_n$ with f_n the natural frequency, the damping factor ζ and the capacitance ratio m, where:

$$(m+2)\cdot\zeta\omega_n T = \frac{\mu_1-\mu_2+\mu_3}{1-\mu_1}, \tag{46}$$

$$(1+2m\zeta^2)\cdot(\omega_n T)^2 = \frac{\mu_2-2\mu_3}{1-\mu_1}, \tag{47}$$

$$m\zeta\cdot(\omega_n T)^3 = \frac{\mu_3}{1-\mu_1}. \tag{48}$$

The capacitance ratio m is an additional factor for third-order PLL used to adjust the step response character [27]. By comparing (44) and (45), (μ_1,μ_2,μ_3) can be expressed by (ω_n,ζ,m) as:

$$\mu_1 = \frac{(m+2)\zeta\omega_n T + (1+2m\zeta^2)(\omega_n T)^2 + m\zeta(\omega_n T)^3}{1+(m+2)\zeta\omega_n T + (1+2m\zeta^2)(\omega_n T)^2 + m\zeta(\omega_n T)^3}, \tag{49}$$

$$\mu_2 = \frac{(1+2m\zeta^2)(\omega_n T)^2 + 2m\zeta(\omega_n T)^3}{1+(m+2)\zeta\omega_n T + (1+2m\zeta^2)(\omega_n T)^2 + m\zeta(\omega_n T)^3}, \tag{50}$$

$$\mu_3 = \frac{m\zeta(\omega_n T)^3}{1+(m+2)\zeta\omega_n T + (1+2m\zeta^2)(\omega_n T)^2 + m\zeta(\omega_n T)^3}. \tag{51}$$

2) Stability: The condition of stability of the causal rational system $L(z)$ is obtained when all the roots of the denominator polynomial are inside the unit circle. In view of the complexity of the third-order transfer function, we resort to a simplified Jury-Marden method [28].

The third-order denominator polynomial of $L(z)$ in (44) is $D(z) = a_0 z^3 + a_1 z^2 + a_2 z + a_3$, with $a_0 = 1$, $a_1 = \mu_1+\mu_2-3$, $a_2 = 3-2\mu_1-\mu_2+\mu_3$, $a_3 = \mu_1 - 1$, the criterion of stability are given by:

- $D(1) > 0$;
- $D(-1) < 0$;
- $a_0 > |a_3|$, $|c_0| > |c_2|$,

with

$$c_0 = \begin{vmatrix} a_0 & a_3 \\ a_3 & a_0 \end{vmatrix}, \quad c_2 = \begin{vmatrix} a_2 & a_3 \\ a_1 & a_0 \end{vmatrix}.$$

[3]The transfer function $L(z)$ w.r.t. ω_n, ζ and m in (45) is same as the one of Or3-CATL in [1], but the relationships between (μ_1,μ_2,μ_3) and (ω_n,ζ,m) are different since the loop filter derived in this paper is different from the one used in [1] (see footnote 2).

After some manipulations, we obtain the condition of stability of the RW3-CATL, *i.e.*, $L(z)$ is stable if and only if:

$$0 < \mu_1 < 2, \tag{52}$$

$$0 < \mu_3 < \mu_1\mu_2, \tag{53}$$

$$4\mu_1 + 2\mu_2 + \mu_3 < 8. \tag{54}$$

We can rewrite $L(z)$ in the frequency-domain, by setting $z = e^{pT}$, with $p = j\omega = j2\pi f$. Assuming slow reaction of the loop during one symbol time T (*i.e.* $f_n T \ll 1$), the digital loop transfer function is close (approximation $z^{-1} \approx 1 - pT$) to the usual third-order low-pass transfer function in analog PLL ([29], eq.(2)(4)):

$$L(e^{pT}) \approx \frac{(m+2)\zeta\omega_n\cdot p^2 + (1+2m\zeta^2)\omega_n^2\cdot p + m\zeta\omega_n^3}{p^3 + (m+2)\zeta\omega_n\cdot p^2 + (1+2m\zeta^2)\omega_n^2\cdot p + m\zeta\omega_n^3}. \tag{55}$$

Fig. 2 shows the magnitude-frequency graph of the RW3-CATL transfer function and the third-order analog PLL transfer function, respectively given by (45) and (55) with different parameters. We can see that in the low-frequency domain ($fT \ll 1$) and for loops with slow reaction ($f_n T \ll 1$), the two transfer functions match very well, and then the analog version gives a good approximation of the RW3-CATL transfer function.

C. Asymptotic mean squared error analysis

From (43) we know that the estimation error is zero-mean, thus the RW3-CATL is an unbiased estimator. By using the definition $\epsilon(z) = \alpha(z) - \hat{\alpha}(z)$, (43) can be re-written as:

$$\epsilon(z) = (1 - L(z))\cdot\alpha(z) - L(z)\cdot \mathrm{w}_{(n)}. \tag{56}$$

The variance of estimation error is therefore divided into two parts. One comes from the variation of the parameter α and the other comes from the loop noise w:

$$\sigma_\epsilon^2 = E\{\epsilon_{(n)}\cdot\epsilon_{(n)}^*\} = \sigma_{\epsilon\alpha}^2 + \sigma_{\epsilon\mathrm{w}}^2. \tag{57}$$

The component $\sigma_{\epsilon\alpha}^2$ (dynamic error variance) results from the high-pass filtering $(1 - L(z))$ of the input CAs $\alpha_{(n)}$, so we have:

$$\sigma_{\epsilon\alpha}^2 = \int_{-\frac{1}{2T}}^{+\frac{1}{2T}} \Gamma_\alpha(f)\cdot|1 - L(e^{j2\pi fT})|^2 df, \tag{58}$$

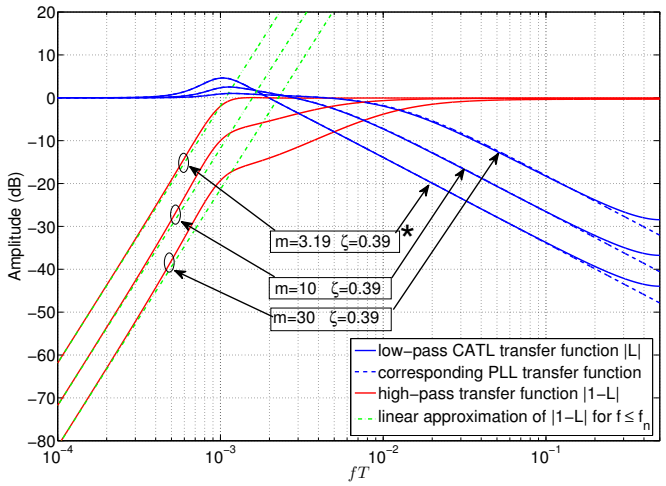

(a) m varies

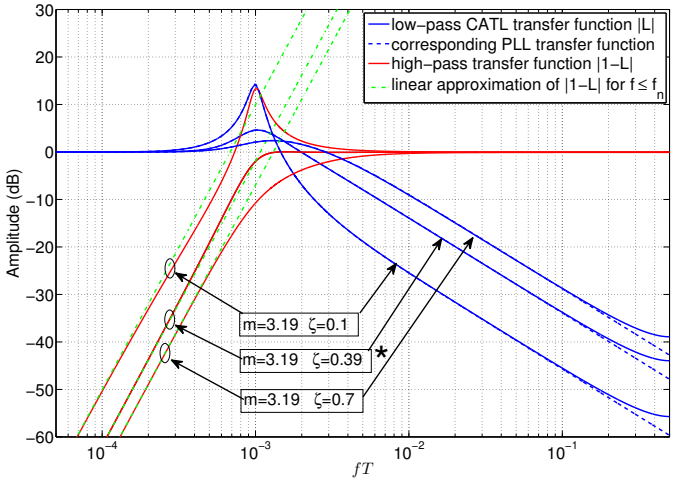

(b) ζ varies

Fig. 2: Transfer functions $|L|$ of RW3-CATL (45) (the three blue continuous curves) and of the corresponding 3rd-order analog PLL (55) (blue dashed curves) versus fT, with fixed natural frequency $f_nT = 10^{-3}$, while varying the parameters (m, ζ) respectively in (a) and (b). Red continuous curves represent the corresponding high-pass transfer function $|1-L|$ and the green dot-dashed lines are the linear approximation defined in (64), the parameters marked by a star ($\star$) are those satisfying the constraint (65)

where $\Gamma_\alpha(f)$ is the power spectral density (PSD) of α given by (2). And the component $\sigma^2_{\epsilon \mathrm{w}}$ (static error variance) results from the low-pass filtering $L(z)$ of the input loop noise $\mathrm{w}_{(n)}$:

$$\sigma^2_{\epsilon \mathrm{w}} = \int_{-\frac{1}{2T}}^{+\frac{1}{2T}} \Gamma_{\mathrm{w}}(f) \cdot |L(e^{j2\pi fT})|^2 df. \tag{59}$$

1) Static error variance $\sigma^2_{\epsilon \mathrm{w}}$: Since the noise is assumed white, the PSD of noise $\Gamma_{\mathrm{w}}(f) = \sigma^2_{\mathrm{w}} T$ is constant all over the system bandwidth. Thus (59) can be rewritten as:

$$\sigma^2_{\epsilon \mathrm{w}} = \sigma^2_{\mathrm{w}} \cdot \underbrace{T \int_{-\frac{1}{2T}}^{+\frac{1}{2T}} |L(e^{j2\pi fT})|^2 df}_{B_L}, \tag{60}$$

where B_L is the so-called equivalent noise bandwidth (double-sided normalized). B_L can be derived ($i.e.$ to evaluate the two-sided complex integral) by using the method presented in [30]. For a third-order system, B_L is a sixth-degree algebraic expression of $\omega_n T$ (see appendix A). But with the condition $f_nT \ll 1$ in our case, the higher order terms than $\omega_n T$ are negligible, so that B_L can be finally approximated as:

$$B_L \approx 2\pi f_n T \cdot \underbrace{\frac{(2m^3\zeta^4 + 12m^2\zeta^4 + 8m\zeta^4 + 6m\zeta^2 + 4\zeta^2 + 1)}{4m^2\zeta^3 + 8m\zeta^3 + 4\zeta}}_{\mathscr{B}}. \tag{61}$$

2) Dynamic error variance $\sigma^2_{\epsilon\alpha}$: The expression for $\sigma^2_{\epsilon\alpha}$ is given by (58) in an integral form. To obtain an analytical expression of $\sigma^2_{\epsilon\alpha}$, the general assumptions $f_d \le f_n \ll 1/T$ is helpful which allows us to do some approximations. By using this assumption, we could approach the term $|1-L(e^{j2\pi fT})|^2$ by two asymptotes (see appendix B for derivation):

$$|1 - L(e^{j2\pi fT})|^2 \approx \begin{cases} \frac{f^6}{(m\zeta)^2 f_n^6} & \text{if} \quad f \ll f_n, \\ 1 & \text{if} \quad f \gg f_n. \end{cases} \tag{62}$$

and for the special point $f = f_n$, we have:

$$|1 - L(e^{j2\pi f_n T})|^2 \approx \frac{f_n^6}{(m\zeta)^2 f_n^6 \; + \; [m^2(4\zeta^2 - 1) + 4].f_n^6}. \tag{63}$$

The two straight asymptotes of the log magnitude in (62) are also evidently shown in Fig.2. Note that the case of $f \gg f_n$ needs not to be taken into account for the integral computation (58), because for the Rayleigh-Jakes model, the spectrum of α, Γ_α, has a bounded support, *i.e.* $|f| \le f_d$, and for a good tracking of α, we assume f_n greater or equal to f_d. So we use the low frequency asymptote for our approximation, yielding:

$$|1 - L(e^{j2\pi fT})|^2 \approx \frac{f^6}{(m\zeta)^2 f_n^6}, \quad \text{if } f \le f_n. \tag{64}$$

And to obtain an acceptable approximation around f_n, we impose that the function $|1 - L(e^{j2\pi fT})|^2$ crosses the low frequency asymptote at $f = f_n$, yielding the following constraint (see (63)):

$$m^2(4\zeta^2 - 1) + 4 = 0. \tag{65}$$

We can see in Fig. 2 that the linear approximation (64) is quite good, especially when the constraint (65) is applied.

Thus the dynamic error variance $\sigma^2_{\epsilon\alpha}$ becomes[4]:

$$\sigma^2_{\epsilon\alpha} \approx \frac{1}{(m\zeta)^2} \int_{-f_d}^{+f_d} \Gamma_\alpha(f) \cdot \left(\frac{f}{f_n}\right)^6 \cdot df. \tag{66}$$

Further more, with the hypothesis that $f \le f_n$, a variable change $\cos(\theta) = (f/f_d)$ permits us to compute an exact analytical solution of the integral (66) as:

$$\sigma^2_{\epsilon\alpha} \approx \frac{5}{16} \cdot \frac{1}{(m\zeta)^2} \cdot \left(\frac{f_d}{f_n}\right)^6 \cdot \sigma^2_\alpha. \tag{67}$$

[4]This formula can be applied in different channel models by changing the complex gain spectrum, *e.g.*, for a 3-D scattering model [31], $\Gamma_\alpha(f)$ becomes a constant which yields a much simpler result

IV. Computation of the RW3-CATL parameters

The MSE of the RW3-CATL σ_ϵ^2 (57) is minimized for a set of optimal parameters (m, ζ, f_n) obtained through a three-dimension optimization. A closed-form analytical expression for this problem can be obtained if we impose the constraint (65), leading to a sub-optimal solution. This constraint minimization is solved with the method of Lagrange multipliers. In section V, we show that the sub-optimal solution yields a performance very close to that of the optimal solution.

By combining (60) and (67), we have now the closed-form expression of the global MSE of the RW3-CATL:

$$\sigma_\epsilon^2(m,\zeta,f_n) = \frac{5}{16}\cdot\frac{1}{(m\zeta)^2}\cdot\left(\frac{f_d}{f_n}\right)^6\cdot\sigma_\alpha^2 \;+\; \sigma_{\mathrm{w}}^2\cdot B_L. \quad (68)$$

For the optimization of (68) over m, ζ and f_n with constraint (65), the auxiliary function to be minimized is given by:

$$J = \frac{5}{16}\cdot\sigma_\alpha^2\cdot\frac{1}{(m\zeta)^2}\cdot\left(\frac{f_d}{f_n}\right)^6+\sigma_{\mathrm{w}}^2\cdot B_L+\lambda\cdot\left[m^2(4\zeta^2-1)+4\right], \quad (69)$$

where λ is the Lagrange multiplier. The detailed computation is given in appendix C, yielding the following sub-optimal parameter values. m is the root of:

$$m^{11}+2m^{10}-16m^9-12m^8+112m^7-176m^6-512m^5+... \\ 448m^4+1024m^3+1024m^2-3072=0, \quad (70)$$

yielding $m \approx 3.19$. ζ is then computed with (65), yielding $\zeta \approx 0.39$, which are slightly different from the values used in [1][5]. Then f_n, which depends on f_d and the SNR $= \frac{\sigma_\alpha^2}{\sigma_{\mathrm{w}}^2}$, is given by:

$$(\frac{f_n}{f_d})(\text{Jakes}) = \left(\frac{5}{64}\cdot\frac{1}{\pi f_d T}\cdot\frac{\sigma_\alpha^2}{\sigma_{\mathrm{w}}^2}\cdot Q\right)^{\frac{1}{7}}, \quad (71)$$

with

$$Q = \frac{1}{m^3\zeta^4\mathscr{D}_m+\zeta^3\mathscr{D}_\zeta}, \quad (72)$$

where $\mathscr{D}_m$ given by (85) and $\mathscr{D}_\zeta$ given by (86) are functions of m and ζ, as defined in Appendix C. Note that the sub-optimal f_n varies as the 7th root of SNR.

Then the sub-optimal MSE can be calculated by:

$$\sigma_\epsilon^2(\text{Jakes}) = C\cdot(\sigma_\alpha^2)^{\frac{1}{7}}\cdot(\sigma_{\mathrm{w}}^2\cdot f_d T)^{\frac{6}{7}}, \quad (73)$$

with

$$C = \left[\frac{2}{(m\zeta)^2}\cdot(\frac{1}{Q})^{\frac{6}{7}} \;+\; \mathscr{B}Q^{\frac{1}{7}}\right]\cdot\left(10\pi^6\right)^{\frac{1}{7}}. \quad (74)$$

[5]Note that in [1], we have used $m = 3, \zeta = 0.37$ as a sub-optimal set, which is obtained from the numerical optimization, and then we proceeded a one-dimension optimization on the natural frequency f_n. Obviously, the Lagrange multiplier approach used here is more accurate because it is a 3-dimension optimization.

V. Simulation

In this section, the performance of the RW3-CATL in terms of MSE and BER is assessed through simulations, and is compared to that of reference algorithms based on KF. For all our simulations the channel autocorrelation function is assumed to be given by the widely accepted Jakes' model, as stated in Section II. Except for Fig. 9, all the results are given in Data-aided mode (with then known pilot symbols).

A. Validation of the theoretical analysis

In the previous section, a method to solve the minimization has been provided, yielding sub-optimal parameters. Now, it remains to check that the MSE obtained with these sub-optimal parameters is close to that obtained with the optimal parameters. We recall that the optimal solution is obtained without taking into account the constraint whereas the sub-optimal solution is obtained with the constraint (65). Note that the optimal solution can be found only by means of numerical optimization. The optimal solution is obtained as follows.

First, we define a domain for m and ζ corresponding to typical practical values for these parameters: $\{0 < m \leqslant 20,\ 0.05 < \zeta < 0.5\}$. For each point of this domain, we calculate by means of a one-dimension numerical optimization the f_n value that minimizes the MSE, and we keep then the value of this minimum MSE. Since f_n depends on SNR and $f_d T$, this numerical computation procedure can be done for various SNR and $f_d T$. As a result, Fig. 3 shows the MSE as a function of m, ζ, computed for SNR = 0 dB and $f_d T = 10^{-3}$. It is noteworthy that there exists a valley-belt in which the lowest MSE values are located. To obtain the set of optimal parameters, it remains to find the global minimum by means of a numerical search. The global minimum is shown in Fig. 3 by a star point. The sub-optimal parameters are also plotted (triangle point). We recall that the sub-optimal parameter values are $m = 3.19$, $\zeta = 0.39$, and for this SNR scenario $f_n/f_d = 2.0$ (f_n is computed with (71)). Note that the sub-optimal point is exactly located on the cross point of the constraint line and the valley-bottom line. The MSE value for the sub-optimal parameters is very closed to that for the optimal parameters, which validates our sub-optimal solution.

Fig. 4 compares the simulated and theoretical MSE versus f_n for $f_d T = 10^{-3}$, and SNR = 0, 20, 40 dB. The sub-optimal loop parameters ($m = 3.19,\ \zeta = 0.39$) are considered (see section IV). The theoretical dynamic and static error variances (dashed lines) $\sigma_{\epsilon\alpha}^2$ and $\sigma_{\epsilon\mathrm{w}}^2$ are obtained by numerical integration of (58) and (59), respectively. The approximated error variances (square points) computed by the approximated formulae ((60) with (61) and (67)) are also plotted. It is observed that the approximated MSEs match very well the theoretical MSEs. On the other hand, we can also observe that the component $\sigma_{\epsilon\alpha}^2$ is the main contribution of σ_ϵ^2 for small f_n, whereas the component $\sigma_{\epsilon\mathrm{w}}^2$ dominates when f_n increases. This is understood from (67) and (61) since $\sigma_{\epsilon\alpha}^2$ is inversely proportional to f_n^6, while $\sigma_{\epsilon\mathrm{w}}^2$ is proportional to f_n.

Simulated MSEs have also been plotted. The simulated dynamic error variance $\sigma_{\epsilon\alpha}^2$ was obtained by forcing the noise $\mathrm{w}_{(n)}$ to zero, whereas the simulated static error variance

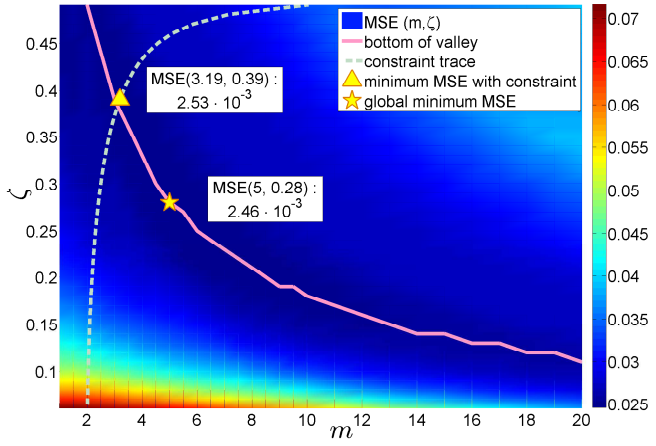

Fig. 3: MSE (57) versus (m, ζ) computed by numerical integration of (58) and (59) with SNR $= 0$ dB, the constraint line is given by (65)

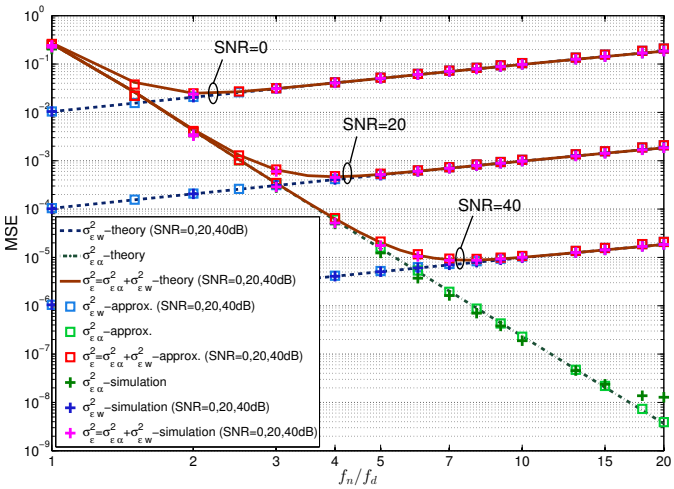

Fig. 4: Theoretical and simulated MSEs versus f_n/f_d (RW3-CATL with $m = 3.19, \zeta = 0.39$, SNR $= 0, 20, 40$ dB, $f_dT = 10^{-3}$)

$\sigma^2_{\epsilon W}$ was obtained by maintaining the CA to a constant. We can observe that all the theoretical curves are very close to the simulated ones too, which validates our theoretical analysis and the approximations. Therefore, the abscissa of the minimum of the simulated MSE σ^2_ϵ also matches very well with the (theoretical closed-form (92)) optimal natural frequency (such that f_n/f_d (Jakes) = 2, 3.9, 7.3 respectively for SNR = 0, 20, 40 dB).

B. Comparison with Kalman estimators in literature

Fig. 5 compares the asymptotic MSE (*i.e.* in tracking mode) of the RW3-CATL with that of the AR1$_{CM}$-KF [5]–[8], the AR1$_{MAV}$-KF [9] [10] and the RW2-KF [11] by means of Monte-Carlo simulations [6] for $f_dT = 10^{-4}$ and $f_dT = 10^{-3}$. Note that our proposed RW3-CATL algorithm assumes the same *a priori* knowledge as that required for the KF (Jakes model, noise variance, Doppler frequency). We also plot the

[6]In this simulation, the results of RW3-KF is not illustrated basically because the steady-state RW3-KF is equivalent to the RW3-CATL, as long as the state noise variance σ^2_u is well tuned, according to Section III-A.

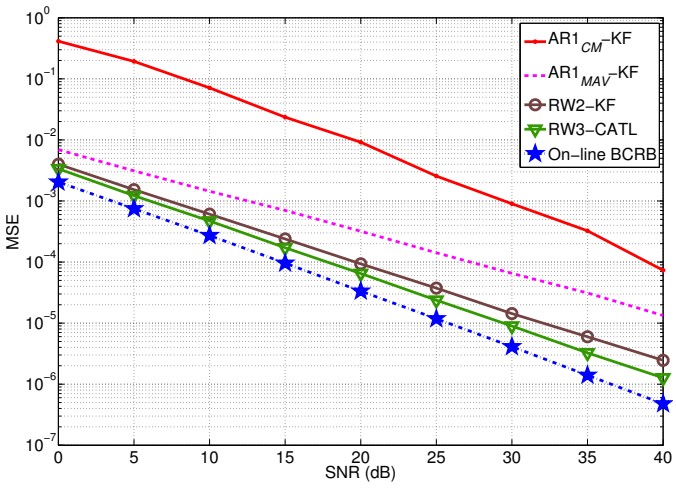

(a) $f_dT = 10^{-4}$

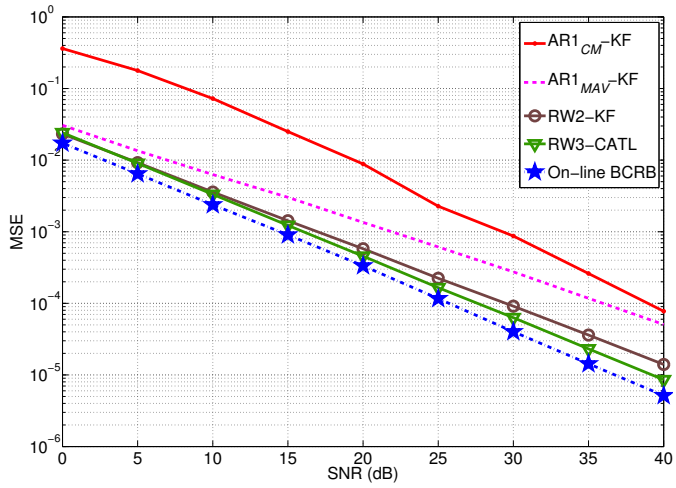

(b) $f_dT = 10^{-3}$

Fig. 5: MSE versus SNR of the RW3-CATL compared to reference estimators, (a) $f_dT = 10^{-4}$ (b) $f_dT = 10^{-3}$

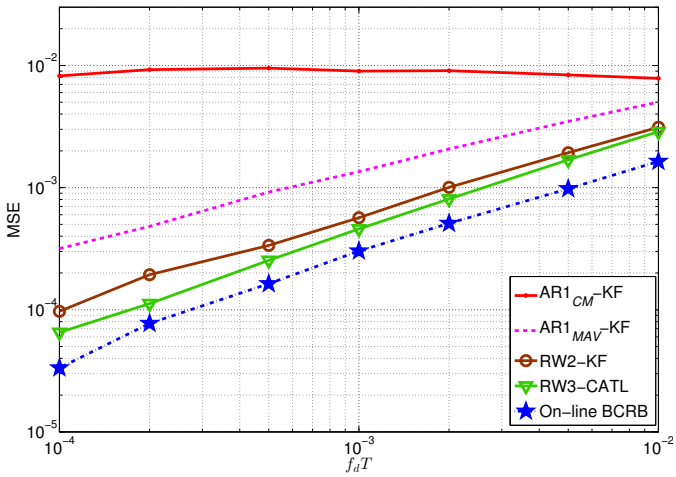

Fig. 6: MSE versus f_dT, SNR $= 20$ dB

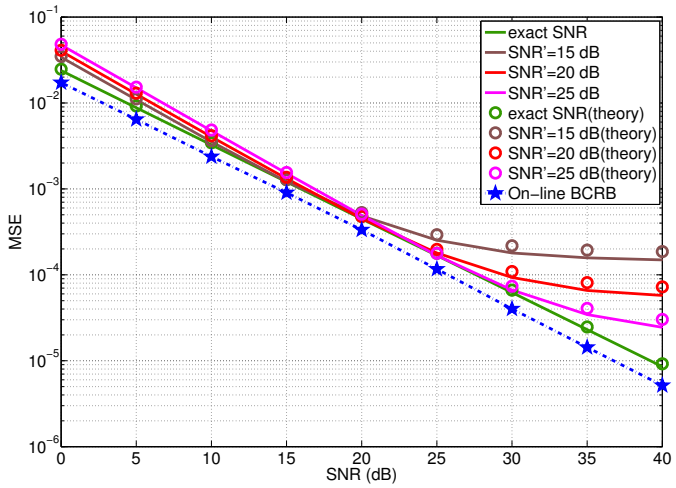

Fig. 7: Effect of a mismatch on the knowledge of SNR : MSE versus SNR, SNR′ (used to tune the RW3-CATL) fixed at 15, 20, 25 dB and $f_dT = 10^{-3}$

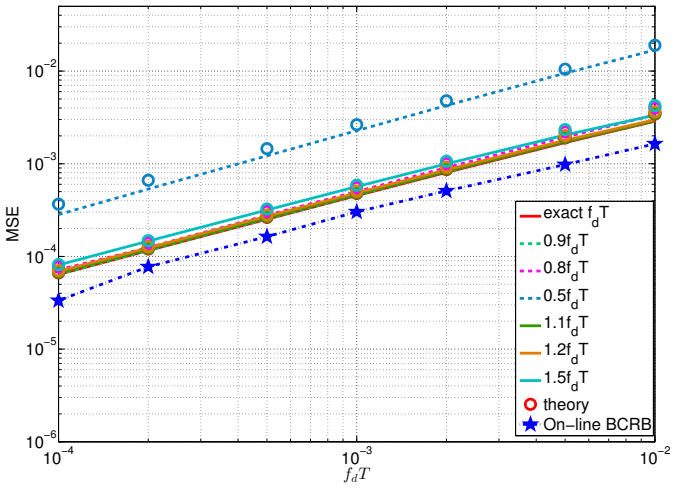

Fig. 8: Effect of a mismatch on the knowledge of f_d : MSE versus f_dT, $f_dT^{'}$ (used to tune the RW3-CATL) shifted 10%, 20%, 50% from the true value and SNR = 20 dB

on-line Bayesian Cramer-Rao bound (BCRB) as reference [32]. It is observed that the asymptotic MSE performance of the AR1$_{CM}$-KF is very poor. This result corroborates the works cited in the introduction, which point out that the AR1$_{CM}$-KF is convenient for high mobility ($f_dT >> 10^{-2}$), but exhibits poor performance at $f_dT \leq 10^{-2}$ as proved by [10]. As expected, the RW2-KF performs better than AR1$_{CM}$-KF and AR1$_{MAV}$-KF. Finally, the asymptotic MSE of the RW3-CATL with the loop parameters properly chosen (see section IV) is the closest to the BCRB (which could be concluded from the MSE expressions of the 4 estimators). This result shows that it is preferable to use a well-chosen third-order algorithm based on simple CATL to a KF when the later is based only on first- or second-order models. According to (73), the theoretical asymptotic MSE of the RW3-CATL is proportional to the $\frac{6}{7}$ power of the noise variance σ_w^2 (note that SNR $= \frac{\sigma_\alpha^2}{\sigma_w^2}$ with here $\sigma_\alpha^2 = 1$ and $\sigma_w^2 < 1$), versus to the $\frac{4}{5}$ and $\frac{2}{3}$ power for the RW2-KF [11] and AR1$_{MAV}$-KF [10] respectively, which is validated by Fig. 5.

Fig. 6 shows the MSE of different systems versus f_dT. The gain in performance of the RW3-CATL is greater for small values of f_dT. When f_dT increases, the MSEs of the AR1$_{MAV}$-KF, RW2-KF and RW3-CATL systems seem to converge to the MSE of the AR1$_{CM}$-KF. This is again understood from (73) that the theoretical asymptotic MSE of the RW3-CATL is proportional to the $\frac{6}{7}$ power of the f_dT.

C. Mismatched design

According to the analysis in section IV, we know that the knowledge of the SNR and f_d is required to design the RW3-CATL parameter f_n. And (68) shows that f_d and the SNR are the two key factors that directly impact the estimation MSE. In this section, we thus depict the sensitivity to imperfect knowledge of SNR and f_d in order to show the robustness of the RW3-CATL. The notation SNR′ and f_d' denote the values of SNR and f_d used to tune the RW3-CATL (not necessarily the correct values). Fig. 7 plots the

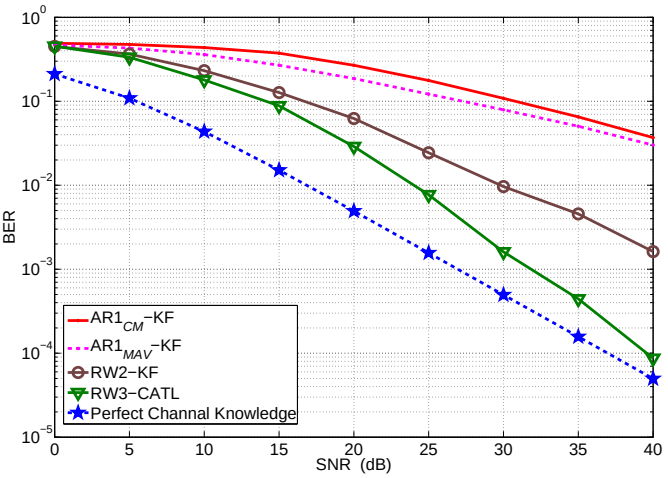

Fig. 9: BER versus SNR for QPSK modulation, $f_dT = 10^{-3}$

MSE versus the true SNR for SNR′ = 15 dB, 20 dB, 25 dB and perfect knowledge of $f_dT = 10^{-3}$ (*i.e.* $f_d' = f_d$), as well as the corresponding theoretical results. It is seen that both overestimation and underestimation of SNR cause performance degradation, and underestimation shows more severe influence. Fig. 8 shows the MSE results of using f_d' with different deviations ($\frac{f_d' - f_d}{f_d} = \pm 10\%, \pm 20\%, \pm 50\%$) and SNR fixed at 20 dB, the corresponding theoretical values are also attached. We also find that, the RW3-CATL can sustain a certain f_d error, for example, within $\pm 20\%$, there is no evident mismatch between the simulation MSE and the optimal MSE. Besides, an underestimated f_d will cause more severe degradation than a same level overestimated f_d, as shown by the $1.5f_d(+50\%)$ and $0.5f_d(-50\%)$ lines in Fig. 8.

D. BER performance

A BER simulation is carried out to evaluate the actual performance of the RW3-CATL estimator. The transmitted

symbols are QPSK modulated. The data frame is composed of 200 continuous pilot symbols and then 1800 unknown symbols. In this context, the channel estimation is in half-blind mode (alternatively by pilots and decisions). Note that the *a priori* decision $\hat{x}_{(n|n-1)}$ is used to compute the error signal (15), but the final decision is computed as: $\hat{x}_{(n)} = \frac{\sqrt{2}}{2} \cdot \text{sgn}\{\mathfrak{Re}(\hat{\alpha}^*_{(n)} \cdot r_{(n)})\} + j\frac{\sqrt{2}}{2} \cdot \text{sgn}\{\mathfrak{Im}(\hat{\alpha}^*_{(n)} \cdot r_{(n)})\}$. Fig. 9 shows that the BER of RW3-CATL remains close to the perfect line (BER with perfect acknowledge of channel) for all SNRs, while the BER of other estimators are further away from the perfect line as SNR increases. We notice also that the classical Kalman estimator based on AR1-model leads to poor BER performance due to the mismatch of AR-1 model, and that this BER can be dramatically reduced in using the *integrated-RW-model-based* estimators (RW2-KF and RW3-CATL). The third-order estimator performs even much better than the second-order one.

VI. Conclusion

In this paper, a channel path complex amplitude estimator over slow to moderate flat fading channels has been proposed. The proposed estimator is based on a third-order tracking loop, which is proved equivalent to a steady-state KF based on a same order integrated random walk (RW) model. The connection between a steady-state KF based on a RW model and the proposed PLL-like estimator is established. This explains the fact that the RW3-CATL can reach in tracking mode the same asymptotic performance as that of a steady-state RW3-KF, even though the former converges slower than the KF. The complete theoretical MSE analysis has been provided. A closed-form formula of the asymptotic MSE as a function of Doppler frequency and SNR is given. We have demonstrated that, by fixing the capacitance ratio to 3.19, the damping factor to 0.39, and by computing the natural frequency with a given expression depending on the Doppler frequency and SNR, it is possible to achieve near-optimal performance in terms of asymptotic MSE. Simulation results (MSE and BER) show that, with these well-chosen parameters, the proposed algorithm outperforms the KF of the literature (based on first- or second-order models), as long as the mobility is moderate (*i.e.* $f_d T < 10^{-2}$), which is a very common scenario. The mismatch simulation shows the robustness of the RW3-CATL in harsh environment test, where the mobility (in terms of f_d) or the background noise power (in terms of SNR) information is distorted. In addition, our proposed algorithm is a computationally less demanding technique than these KF-based algorithms, since it does not require to compute the coefficients at each time period. The simple case of a flat fading channel was considered in this article, but the results can be applied or generalized to more complex systems, such as wireless OFDM systems.

Appendix A
Equivalent Noise Bandwidth of RW3-CATL

Using the result of [30], the two-sided complex integral in the form of (60) could be evaluated by the solution of a closed matrix equation. The matrices are composed by the coefficients of numerator and denominator of the integrand. The transfer function of a third-order system:

$$L(z) = \frac{b_0 z^3 + b_1 z^2 + b_2 z + b_3}{a_0 z^3 + a_1 z^2 + a_2 z + a_3}, \tag{75}$$

then the corresponding matrix equation is given by:

$$\begin{bmatrix} a_0 & a_1 & a_2 & a_3 \\ a_1 & a_0 + a_2 & a_1 + a_3 & a_0 \\ a_2 & a_3 & a_0 & a_1 \\ a_3 & 0 & 0 & a_0 \end{bmatrix} \begin{bmatrix} a_0 B_L \\ M_1 \\ M_2 \\ M_3 \end{bmatrix} = \begin{bmatrix} b_0^2 + b_1^2 + b_2^2 + b_3^2 \\ 2(b_0 b_1 + b_1 b_2 + b_2 b_3) \\ 2(b_0 b_2 + b_1 b_3) \\ 2 b_0 b_3 \end{bmatrix}. \tag{76}$$

In our case, we have from (44) that $b_0 = \mu_1$, $b_1 = -2\mu_1 + \mu_2 + \mu_3$, $b_2 = \mu_1 - \mu_2$, $b_3 = 0$, $a_0 = 1$, $a_1 = \mu_1 + \mu_2 + \mu_3 - 3$, $a_2 = 3 - 2\mu_1 - \mu_2$, $a_3 = \mu_1 - 1$. Combining with (49), (50), (51) leads to (77), where:

$$\begin{aligned}
A &= m^3\zeta^3, \\
B &= 8m^3\zeta^4 + 4m^2\zeta^2, \\
C &= 20m^3\zeta^5 + 5m^3\zeta^3 + 30m^2\zeta^3 + 5m\zeta, \\
D &= 16m^3\zeta^6 + 22m^3\zeta^4 + 68m^2\zeta^4 + 16m^2\zeta^2 + 34m\zeta^2 + 2, \\
E &= 24m^3\zeta^5 + 4m^3\zeta^3 + 48m^2\zeta^5 + 56m^2\zeta^3 + 64m\zeta^3 + 14m\zeta + 12\zeta, \\
F &= 8m^3\zeta^4 + 48m^2\zeta^4 + 32m\zeta^4 + 24m\zeta^2 + 16\zeta^2 + 4, \\
G &= 16m^3\zeta^6 + 22m^3\zeta^4 + 68m^2\zeta^4 + 18m^2\zeta^2 + 34m\zeta^2 + 2, \\
H &= 24m^3\zeta^5 + 4m^3\zeta^3 + 48m^2\zeta^5 + 68m^2\zeta^3 + 64m\zeta^3 + 20m\zeta + 12\zeta, \\
I &= 8m^3\zeta^4 + 64m^2\zeta^4 + 8m^2\zeta^2 + 32m\zeta^4 + 56m\zeta^2 + 16\zeta^2 + 8, \\
J &= 16m^2\zeta^3 + 32m\zeta^3 + 16\zeta.
\end{aligned}$$

Appendix B
Asymptote approximation of $|1 - L(e^{j2\pi fT})|^2$

Under the general assumption $f_n \ll 1/T$, the squared modulus of the high pass-filter $1 - L$ can be written from (55) as:

$$\begin{aligned}
&|1 - L(e^{j2\pi fT})|^2 \qquad \text{(for } |f| \ll 1/T\text{)} \\
&= f^6 / \left\{ m^2\zeta^2 f_n^6 + [(m+2)^2\zeta^2 - 2(1 + 2m\zeta^2)] f_n^2 f^4 + \cdots \right. \\
&\qquad \left. [(1 + 2m\zeta^2)^2 - 2(m^2 + 2m)\zeta^2] f_n^4 f^2 + f^6 \right\}.
\end{aligned} \tag{78}$$

The red curves in Fig. 2 shows the magnitude of $|1 - L(e^{j2\pi fT})|^2$ as a function of f for different values of m and ζ and for $f_n T = 10^{-3}$. Note that with the form in (78), the integral (60) is too tedious to derive. In order to obtain an

$$B_L = \frac{A(\omega_n T)^6 + B(\omega_n T)^5 + C(\omega_n T)^4 + D(\omega_n T)^3 + E(\omega_n T)^2 + F(\omega_n T)}{A(\omega_n T)^6 + B(\omega_n T)^5 + C(\omega_n T)^4 + G(\omega_n T)^3 + H(\omega_n T)^2 + I(\omega_n T) + J} \tag{77}$$

analytical expression of the integral, it is necessary to simplify the expression of $|1 - L(e^{j2\pi fT})|^2$.

For that purpose, let us consider the asymptotic behaviour of the log magnitude as a function of frequency. At low frequencies, *i.e.* $f \ll f_n$, we get $f_n^2 f^4 \ll f_n^6$ and $f^6 \ll f_n^6$, yielding:

$$\begin{aligned} m^2\zeta^2 f_n^6 + [(m+2)^2\zeta^2 - 2(1+2m\zeta^2)] f_n^2 f^4 + ... \\ [(1+2m\zeta^2)^2 - 2(m^2+2m)\zeta^2] f_n^4 f^2 + f^6 \\ \approx (m\zeta)^2 f_n^6. \end{aligned} \quad (79)$$

At high frequencies, i.e. $f \gg f_n$, we get:

$$\begin{aligned} m^2\zeta^2 f_n^6 + [(m+2)^2\zeta^2 - 2(1+2m\zeta^2)] f_n^2 f^4 + ... \\ [(1+2m\zeta^2)^2 - 2(m^2+2m)\zeta^2] f_n^4 f^2 + f^6 \\ \approx f^6. \end{aligned} \quad (80)$$

By combining (79) and (80), we obtain thus (62). Then, by using $f = f_n$, (63) is found directly from (78).

Appendix C
Minimization of Asymptotic MSE with Lagrange multipliers method

We apply the method of Lagrange multipliers to minimize (68) with constraint (65). Given the auxiliary function, the problem reduces to solve the following system of equations:

$$\begin{cases} \dfrac{\partial J}{\partial f_n} = 2\pi\sigma_{\mathrm{w}}^2 T\mathscr{B} - \dfrac{15}{8}\cdot\dfrac{1}{(m\zeta)^2}\cdot\sigma_\alpha^2\cdot\dfrac{f_d^6}{f_n^7} = 0, & (81) \\ \dfrac{\partial J}{\partial m} = 2\pi\sigma_{\mathrm{w}}^2 T f_n\mathscr{D}_m - \dfrac{5}{8}\cdot\sigma_\alpha^2\cdot\left(\dfrac{f_d}{f_n}\right)^6\cdot\dfrac{1}{\zeta^2 m^3} \\ \qquad + 2\lambda(4\zeta^2-1)m = 0, & (82) \\ \dfrac{\partial J}{\partial \zeta} = 2\pi\sigma_{\mathrm{w}}^2 T f_n\mathscr{D}_\zeta - \dfrac{5}{8}\cdot\sigma_\alpha^2\cdot\left(\dfrac{f_d}{f_n}\right)^6\cdot\dfrac{1}{m^2\zeta^3} \\ \qquad + 8\lambda m^2\zeta = 0, & (83) \\ m^2(4\zeta^2-1) + 4 = 0, & (84) \end{cases}$$

with

$$\begin{aligned} \mathscr{D}_m =& \frac{\partial\mathscr{B}}{\partial m} \\ =& \frac{m^4\zeta^5 + 4m^3\zeta^5 + 8m^2\zeta^5 + 8m\zeta^3 - m\zeta + 2\zeta}{2m^4\zeta^4 + 8m^3\zeta^4 + 8m^2\zeta^4 + 4m^2\zeta^2 + 8m\zeta^2 + 2}, \end{aligned} \quad (85)$$

$$\begin{aligned} \mathscr{D}_\zeta =& \frac{\partial\mathscr{B}}{\partial\zeta} \\ =& \frac{2m^5\zeta^6 + 16m^4\zeta^6 + 32m^3\zeta^6 + 16m^2\zeta^6 + \cdots}{4m^4\zeta^6 + 16m^3\zeta^6 + 16m^2\zeta^6 + 8m^2\zeta^4 + 16m\zeta^4 + 4\zeta^2} \\ & \frac{\cdots + 20m^2\zeta^4 - 3m^2\zeta^2 + 16m\zeta^4 + 4\zeta^2 - 1}{}. \end{aligned} \quad (86)$$

Since m and ζ are real positive parameters, from (84) we have:

$$\zeta = \frac{\sqrt{(m^2-4)}}{2m}, \quad (87)$$

which indicates that $m > 2$. Replace all the ζ in (81), the system of equations becomes:

$$\begin{cases} C_1\mathscr{B}' - \dfrac{6C_2}{f_n^7\cdot\frac{m^2-4}{4}} = 0, & (88) \\ C_1\mathscr{D}_m' f_n - \dfrac{2C_2}{f_n^6\cdot\frac{m(m^2-4)}{4}} - \dfrac{8\lambda}{m} = 0, & (89) \\ C_1\mathscr{D}_\zeta' f_n\cdot\dfrac{\sqrt{(m^2-4)}}{2m} - \dfrac{2C_2}{f_n^6\cdot\frac{m^2-4}{4}} \\ \qquad + 2\lambda(m^2-4) = 0, & (90) \end{cases}$$

with $C_1 = 2\pi\sigma_{\mathrm{w}}^2 T$ and $C_2 = \frac{5}{16}\cdot f_d^6\cdot\sigma_\alpha^2$. The terms $\mathscr{B}'$, $\mathscr{D}_m'$ and $\mathscr{D}_\zeta'$ are respectively obtained from $\mathscr{B}$ (61), $\mathscr{D}_m$ (85) and $\mathscr{D}_\zeta$ (86) where ζ is replaced by (87). Then by combining (89) and (90), λ and f_n can be expressed as a function of m as follows:

$$\lambda = \frac{1}{8}C_1\mathscr{D}_m' f_n m - \frac{C_2}{f_n^6\cdot(m^2-4)}, \quad (91)$$

$$f_n = \left(\frac{8C_2m^3}{C_1(m^2-4)\left[\mathscr{D}_m' m^2(m^2-4) + 2\mathscr{D}_\zeta'\sqrt{(m^2-4)}\right]}\right)^{\frac{1}{7}}. \quad (92)$$

Finally, by using (92), we do some manipulations with (88), the system of equations reduces to (70), this equation has 11 roots that we can obtain by Computer-aided calculation. The condition of m (real positive and $m > 2$) returns a unique available value, that is $m = 3.19$. We obtained then $\zeta = 0.39$ by (87), and also f_n by (92).

References

[1] Shu, H., Ros, L., and Simon, E.P.: 'Third-order complex amplitudes tracking loop for slow fading channel estimation', Proc. 19th International Conference on Telecommunications (ICT), Jounieh, Lebanon, April 2012, pp. 1–6.

[2] Jakes, W.C.: 'Microwave Mobile Communications', New-York: John Wiley, 1974.

[3] Clarke, R.H.: 'A statistical theory of mobile radio reception', Bell System Technical Journal, July 1968, vol. 47, pp. 957–1000.

[4] Baddour. K., Beaulieu. N.: 'Autoregressive modeling for fading channel simulation', IEEE Trans. Wireless Commun., July 2005, vol. 4, no. 4, pp. 1650–1662.

[5] Komninakis, C., Fragouli, C., Sayed, A., Wesel, R.: 'Multi-input multi-output fading channel tracking and equalization using Kalman estimation', IEEE Trans. Signal Process., May 2002, vol. 50, no. 5, pp. 1065–1076.

[6] Liu, Z., Ma, X., Giannakis, G.: 'Space-time coding and Kalman filtering for time-selective fading channels', IEEE Trans. Commun., Feb. 2002, vol. 50, no. 2, pp. 183–186.

[7] Chen, W., Zhang, R.: 'Kalman-filter channel estimator for OFDM systems in time and frequency-selective fading environment', Proc. IEEE Int. Conf. Acoust. Speech Signal Process., May 2004, vol. 4, pp. iv–377–iv–380.

[8] Al-Naffouri, T.: 'An EM-Based Forward-Backward Kalman Filter for the Estimation of Time-Variant Channels in OFDM', IEEE Trans. Signal Process., 2007, vol. 55, no. 7, pp. 3924–3930.

[9] Barbieri, A., Piemontese, A., Colavolpe, G.: 'On the ARMA approximation for fading channels described by the Clarke model with applications to Kalman-based receivers', IEEE Trans. Wireless Commun., 2009, vol. 8, no. 2, pp. 535–540.

[10] Ghandour-Haidar, S., Ros, L., Brossier, J.-M.: 'On the use of first-order autoregressive modeling for Rayleigh flat fading channel estimation with Kalman filter', ELSEVIER Signal Processing, 2012, vol. 92, no. 2, pp. 601–606.

[11] Ros, L., Simon, E.P.: 'Second-order modeling for Rayleigh flat fading channel estimation with Kalman Filter', Proc. 17th Int. Conf. Digital Signal Process., 2011, pp. 1–6.

[12] Wang, H., Chang, P.: 'On veryfying the first-order Markovian assumption for a Rayleigh fading channel model', IEEE Trans. veh. Technol., 1996, vol.45, pp. 353–357.

[13] Hijazi, H., Ros, L.: 'Joint data QR-detection and Kalman estimation for OFDM time-varying Rayleigh channel complex gains', IEEE Trans. Commun., Jan. 2010, vol. 58, no. 1, pp. 170–178.

[14] Simon, E.P., Ros, L., Hijazi, H., Ghogho, M.: 'Joint Carrier Frequency Offset and Channel Estimation for OFDM Systems via the EM Algorithm in the Presence of Very High Mobility', IEEE Trans. Signal Process., Feb. 2012, vol. 60, no. 2, pp. 754–765.

[15] Tugnait, J., He, S., Kim, H.: 'Doubly selective channel estimation using exponential basis models and subblock tracking', IEEE Trans. Signal Process., 2010, vol. 58, no. 3, pp. 1275–1289.

[16] Ros, L., Hijazi, H., Simon, E.P.: 'Paths complex gain tracking algorithms for ofdm receiver in slowly-varying channels', Proc. 4th Int. Symp. Commun. Control and Signal Process. (ISCCSP), Mar. 2010, pp. 1–6.

[17] Lindbom, L., Sternad, M., Ahlen, A.: 'Tracking of time-varying mobile radio channels .1. the wiener lms algorithm', IEEE Trans. Commun., Dec. 2001, vol. 49, no. 12, pp. 2207–2217.

[18] Gazor, S.: 'Prediction in LMS-type adaptive algorithms for smoothly time varying environments', IEEE Trans. Signal Process., June 1999, vol. 47, no. 6, pp. 1735 –1739.

[19] Xue, Y., Zhu, X.: 'Second-order LMS based wireless channel tracking: implementation under imperfect carrier synchronization', ELSEVIER Signal Process., Jan. 2003, vol. 83, no. 1, pp. 199–212.

[20] Ros, L., Hijazi, H., Simon, E.P.: 'Complex amplitudes tracking loop for multipath slow fading channel estimation in OFDM systems', (Research Report, Gipsa-lab, April 2012)

[21] Driessen, P.: 'DPLL bit synchronizer with rapid acquisition using adaptive Kalman filtering techniques', IEEE Trans. Commun., Sept. 1994, vol. 42, no. 9, pp. 2673 –2675.

[22] Christiansen, G.: 'Modeling of PRML timing loop as a Kalman filter', Proc. IEEE Global Telecommun. Conf. (GLOBECOM), 1994, vol. 2, pp. 1157–1161.

[23] Patapoutian, A.: 'On phase-locked loops and Kalman filters', IEEE Trans. Commun., May 1999, vol. 47, no. 5, pp. 670–672.

[24] Kay, S.M.: 'Fundamentals of Statistical Signal Processing: Estimation Theory', Prentice Hall PTR, April 1993.

[25] K. Chui, G., Chen, G.: 'Kalman Filtering with real-time applications (4th edition)'. Springer-Verlag, 2000.

[26] Lindsey, W., Chie, C.M.: 'A survey of digital phase-locked loops', Proc. of the IEEE, 1981, vol. 69, no. 4, pp. 410–431.

[27] Hu, S.: 'Principle of Automatic Control (4th edition)', Beijing: Science Press, 2001.

[28] Antoniou, A.: 'Digital Signal Processing', McGraw-Hill, 2005.

[29] Shan, C., Chen, Z., Zhu, L., Li, Y.: 'Design and Implementation of Bandwidth Adaptable Third-Order All Digital Phase-Locked Loops', Proc. 6th Int. Conf. Wireless Commun. Networking and Mobile Computing (WiCOM), 2010, pp. 1–4.

[30] Winkelstein, R.: 'Closed form evaluation of symmetric two-sided complex integrals', TDA Progress Report, 1981.

[31] Clarke, R., Khoo, W.L.: '3-D mobile radio channel statistics', IEEE Trans. Veh. Technol., Aug. 1997, vol. 46, no. 3, pp. 798–799.

[32] Hijazi, H., Ros, L.: 'Bayesian Cramer-Rao Bounds for complex gain parameters estimation of slowly varying Rayleigh channel in OFDM systems', ELSEVIER Signal Process., 2009, vol. 89, no. 1, pp. 111–115.